Journal of Catalysis 280 (2011) 116–124

Contents lists available at ScienceDirect

Journal of Catalysis

journal homepage: www.elsevier.com/locate/jcat

Mechanistic origins of the promoting effect of tiny amounts of Rh on the performance of NiO_x/Al_2O_3 in partial oxidation of methane

Claudia Berger-Karin, Jörg Radnik, Evgenii V. Kondratenko *

Leibniz Institute for Catalysis at the University of Rostock, Albert-Einstein-Str. 29A, D-18059 Rostock, Germany

ARTICLE INFO

Article history:
Received 15 January 2011
Revised 11 March 2011
Accepted 12 March 2011
Available online 14 April 2011

Keywords:
Methane
Oxidation
Syngas
Nickel
Rhodium
TAP reactor
Mechanism

ABSTRACT

The influence of Rh concentration (0.005–0.15 wt.%) in NiO_x(3 wt.%)/Al_2O_3 on the mechanism and kinetics of partial oxidation of methane (POM) to syngas was elucidated by combining steady-state catalytic tests over 120 h on stream with catalysts characterization and temporal analysis of products. All bi-metallic catalysts showed POM performance close to the thermodynamic one. The reaction mechanism does not depend on the nature of metals but is influenced by their reduction state. From a kinetic point of view, rhodium species (both reduced and oxidized) possess significantly higher activity toward methane conversion than the nickel ones. Rhodium fulfills a double role in the bi-metallic catalysts. Irrespective of its concentration, it promotes the reduction of Ni^{2+} in inactive $NiAl_xO_y$ to metallic Ni directly under POM conditions. This is a reason for the higher activity and selectivity of low Rh-loaded (0.005 wt.%) NiO_x(3 wt.%)/Al_2O_3 catalyst compared to its respective mono-metallic counterparts. Owing to the high activity of rhodium species, they alone determine the POM performance of higher Rh-loaded catalysts.

1. Introduction

The modern chemical industry is mainly based on crude oil as a raw feedstock. Natural gas, the reserves of which are estimated to exceed those of crude oil, may be considered now and, particularly, in the future as a preferable raw material replacing crude oil for various purposes. Therefore, a strong economical interest exists in converting natural gas consisting mainly of methane to value added products. An important industrial utilization of methane is the production of hydrocyanic acid via the Andrussow or Degussa processes using Pt and Rh as catalytic materials [1]. Steam and autothermal reforming of methane over nickel-based supported catalysts is a mature technology for producing syngas ($CO + H_2$). The latter is further used for the methanol [2] or Fischer–Tropsch syntheses [3].

Even though the methane reforming reactions are well optimized, there are economic needs for their further improvement with respect to catalyst activity, ratio of H_2:CO, resistance against deactivation via coking and poisoning by sulfur compounds [4]. Partial oxidation of methane (POM) is an attractive alternative because it is exothermal and results in the H_2:CO ratio of 2, which is required for the above syngas functionalizations. The POM reaction has been intensively investigated in the past [5]. Supported nickel catalysts were found to be active but suffer from fast deactivation caused by coke formation as well as sintering of nickel particles. In comparison, noble metal (Pt, Pd, Ir, Ru, and Rh) catalysts exhibit higher activity and time-on-stream stability. However, they are much more expensive compared to nickel.

Taking into account the pivotal importance of syngas in the modern and future chemical industry, cheap, thermally resistant, and stable catalysts would significantly improve the economy of syngas production [6]. Several earlier studies reported on an increase in the activity and time-on-stream stability of Ni-based catalysts when promoting them with small amounts ($\geqslant$0.05 wt.%) of noble metals [7,8]. In general, it was suggested that the presence of noble metals assists (i) to maintain a higher amount of nickel in the metallic state by hydrogen spillover [9–12], (ii) to increase the rate of methane decomposition, being the rate-limiting step [13], and (iii) to promote the formation of smaller initial nickel particles showing higher time-on-stream stability [14].

Very recently, Enger et al. [15] demonstrated that the light-off temperature in the short-contact time POM reaction under temperature-programmed conditions shifted to lower temperatures upon promoting a low-loaded alumina-supported Ni (0.5 wt.%) catalyst with traces of Rh, Ru, or Pt (0.005 wt.%). However, the activity and syngas selectivity of the bi-metallic catalysts did not significantly differ from those of the Rh mono-metallic ones and were lower than the equilibrium values at 1073 K (highest furnace temperature in their experiments). It also should be stressed that the latter experiments were performed under conditions where a severe temperature gradient in the catalyst bed can be expected. Therefore, it was challenging to perform any detailed mechanistic analysis. Enger et al. [15] also stated that the catalyst precursors must be activated by in situ reduction in hydrogen, which

* Corresponding author. Fax: +49 (0) 381 1281 51290.
E-mail address: evgenii.kondratenko@catalysis.de (E.V. Kondratenko).

0021-9517/$ - see front matter © 2011 Elsevier Inc. All rights reserved.
doi:10.1016/j.jcat.2011.03.010

constitutes a restriction for a possible industrial application of such materials. In the present study, we demonstrate that alumina-supported bi-metallic catalysts with low loadings of Ni (3 wt.%) and Rh ($\geqslant$0.005 wt.%) are active and selective for syngas production via POM without any reductive activation. For example, they showed a near-to-equilibrium performance (X(CH_4) = 95%, S(CO) = 91%, and S(H_2) = 97%) at 1073 K. No visible catalyst deactivation was observed during at least 120 h on stream. The presence of tiny amounts of Rh in NiO_x(3 wt.%)/Al_2O_3 is an essential requirement for an efficient production of syngas because the corresponding mono-metallic catalysts were significantly less active and selective.

Based on the above background, the aim of this article was to elucidate mechanistic origins of the promoting effect of Rh ($\geqslant$0.005 wt.%) on a level as elementary as possible. Such knowledge is of prime importance for tailored catalyst development. Since commonly used spectroscopic techniques are not applicable for the in situ analysis of such low metal loadings, particularly at high reaction temperatures, we applied the temporal analysis of products (TAP) reactor for catalyst characterization at 1073 K, i.e., reaction temperature of steady-state ambient pressure POM tests. This technique was demonstrated to be an excellent tool for mechanistic analysis of high-temperature ammonia oxidation to nitric oxide [16,17] and ammonia coupling with methane to hydrocyanic acid [18,19] under isothermal conditions. In order to identify common factors influencing selectivity and activity of the studied catalysts, the derived mechanistic knowledge was related to physico-chemical properties of mono- and bi-metallic catalysts. The catalysts before and after the POM reaction were additionally characterized by XRD, X-ray photoelectron spectroscopy (XPS), and diffuse reflectance UV/Vis (UV/Vis-DR) spectroscopy.

2. Experimental

2.1. Catalyst preparation

Incipient wetness impregnation method [20] was applied for catalyst preparation. Commercial γ-Al_2O_3 (NWa-155, provided by SASOL) was used as support material. It was impregnated with aqueous solutions of nickel and/or rhodium nitrates at room temperature to yield mono- and bi-metallic catalyst precursors. The impregnated materials were dried at 383 K for 2 h followed by their calcination in a muffle furnace at 1073 K for 4 h in static air. The final catalysts are denoted by their weight concentrations of nickel and rhodium, i.e., the metal loading (in wt.%) is given directly prior to the element symbols (e.g., 3Ni_0.005Rh). The endings "_red" and "_used" were added after catalyst abbreviation to distinguish the fresh materials (Tables 1 and 2) from those having been pre-reduced or used in the POM reaction for 120 h, respectively.

2.2. Catalyst characterization

In order to evaluate catalysts microstructure, elemental composition, surface composition, and specific surface areas, the catalytic materials were characterized by XRD, XPS, inductively coupled plasma optical emission spectroscopy (ICP-OES), and nitrogen adsorption technique, as well as UV/Vis-DR spectroscopy. Brief descriptions of each of the characterization methods and experimental procedures are given below.

ICP-OES (Varian 715-ES setup) was used to determine the nickel and rhodium content of each catalyst after calcination at 1073 K. The final metal contents as well as selected physico-chemical properties of catalytic materials are presented in Table 1.

X-ray diffractograms were recorded on a STOE Stadi P diffractometer using Cu Kα radiation (λ = 0.154 nm). Diffraction patterns were collected in the Bragg angle (2θ) range from 15° to 60°.

X-ray photoelectron spectra were acquired using a VG ESCALAB setup up from VG Scientific. A monochromatic Al Kα X-ray anode (1486.6 eV) was applied for exciting core-level electrons to leave the material. Binding energies (E_B) were related to the C1s peak (284.8 eV) according to the National Institute of Standards and Technologies. In order to quantify the oxidation state of nickel before and after the POM reaction, its valence state was determined from the Ni2$p_{3/2}$ peaks. To this end, they were fitted with Gaussian–Lorentzian curves. The resulting peak areas, the specific Scofield factors, and the transmission function of the spectrometer were applied for calculating the concentrations. The modified Auger parameter α, which is useful to unambiguously identify the oxidation state of nickel, was calculated according to Eq. (1) as suggested by Wagmer et al. [21].

$$\alpha = E_{kin}(NiL_3M_{45}M_{45}) + E_B(Ni2p_{3/2}) \quad (1)$$

where E_{kin}($NiL_3M_{45}M_{45}$) and E_B(Ni2$p_{3/2}$) are kinetic and binding energies, respectively.

Nitrogen physisorption at 77 K on BELSORP-mini II setup (BEL Japan, Inc.) was employed to determine specific surface areas according to the Brunauer–Emmet–Teller (BET) equation.

Table 2
Steady-state performance of non-reduced and pre-reduced catalytic materials in the partial oxidation of methane at 1073 K using a CH_4:O_2:N_2 = 2:1:4 feed with GHSV of 24,640 h^{-1}. Catalyst pre-reduction was performed at 1073 K for 1 h in a flow of 10% H_2 in N_2 with GHSV of 15,455 h^{-1}.

Catalysts	X(CH_4) (%)		S(CO) (%)		S(CO_2) (%)		S(H_2) (%)	
	1st cycle	2nd cycle	1st cycle	2nd cycle	1st cycle	2nd cycle	1st cycle	2nd cycle
Non-reduced catalysts								
3Ni	33.7	34.3	43.2	44.4	56.8	55.2	68.0	70.3
0.005Rh	47.3	43.9	78.8	79.2	17.3	18.6	79.0	76.3
3Ni_0.005Rh	89.2	95.4	88.1	90.8	4.2	1.9	91.8	97.1
0.03Rh	95.3	95.3	90.2	90.5	2.1	2.2	96.3	97.4
3Ni_0.03Rh	96.5	96.4	90.9	91.3	1.7	1.5	96.9	97.9
0.15Rh	96.5	96.5	90.9	91.0	1.7	1.5	96.3	96.9
3Ni_0.15Rh	96.4	96.4	90.8	91.0	1.7	1.8	96.4	97.2
Pre-reduced catalysts								
3Ni_red	94.4		94.0		4.5		97.9	
0.005Rh_red	76.6		87.9		11.5		88.4	
3Ni_0.005Rh_red	95.1		94.7		4.0		100.0	

Table 1
Catalysts composition and their specific surface areas.

Catalysts	Abbreviation	Ni (wt.%)	Rh (wt.%)	XRD composition	S_{BET} (m^2 g^{-1})
$Ni_{0.03}Al_2O_3$	3Ni	3.2		Al_2O_3 + $NiAl_xO_y$	118
$Rh_{0.00005}Al_2O_3$	0.005Rh		0.005	Al_2O_3	114
$Ni_{0.03}Rh_{0.00005}Al_2O_3$	3Ni_0.005Rh	3.1	0.005	Al_2O_3 + $NiAl_xO_y$	121
$Rh_{0.0003}Al_2O_3$	0.03Rh		0.03	Al_2O_3	103
$Ni_{0.03}Rh_{0.0003}Al_2O_3$	3Ni_0.03Rh	3.1	0.03	Al_2O_3 + $NiAl_xO_y$	105
$Rh_{0.0015}Al_2O_3$	0.15Rh		0.15	Al_2O_3	105
$Ni_{0.03}Rh_{0.0015}Al_2O_3$	3Ni_0.15Rh	3.1	0.15	Al_2O_3 + $NiAl_xO_y$	105

UV/Vis-DR analysis was performed at room temperature with fresh samples (calcined at 1073 K) using an AVASPEC fiber optical spectrometer (Avantes) equipped with a DH-2000 deuterium–halogen light source and a CCD array detector. $BaSO_4$ was used as a white reference material.

2.3. Catalytic tests

Catalytic tests on the POM reaction were carried out in a multi-channel reactor system at atmospheric pressure using a methane and air feed in a stoichiometric CH_4:O_2 ratio of 2. This setup consists of 48 plug flow fixed-bed quartz reactors (reactor i.d. = 4 mm) operating in parallel. Thirty milligrams of the fresh catalyst (sieve fraction of 250–500 μm) was filled into each reactor. An in-house developed flow restrictor equally distributed the total gas flow to 48 reactors with a constant gas-hourly space velocity (GHSV) of 24,640 h^{-1} per reactor.

Two cycles of the POM reaction were performed according to the following protocol. Initially, the catalysts were heated up to 873 K in Ar flow. Hereafter, the methane–air mixture was fed to the reactors at the same temperature followed by increasing the temperature to 1073 K in 50–100 K increments. The temperature was held constant at each setting for at least 12 h. After the tests at 1073 K, the samples were cooled down to 873 K in Ar flow, and a second measuring cycle was conducted. The POM reaction was studied at this temperature for 25 h on stream. Adjacently, the tests were performed at 973 K and 1073 K for 12 and 20 h on stream, respectively. In total, the catalysts were exposed to the POM feed for 120 h.

In order to analyze the effect of catalysts pre-reduction by H_2 on their POM performance, catalytic experiments were conducted in a six-channel parallel apparatus (quartz reactor i.d. = 6 mm) as follows. Sixty milligrams of the catalyst (sieve fraction of 250–500 μm) was filled into each reactor. The samples were heated in Ar flow to 1073 K, and then the feed was switched to a reduction mixture consisting of 10% H_2 in N_2 with a total GHSV of 15,455 h^{-1}. After the catalysts reduction for 1 h, the reducing feed was switched to Ar flow and the temperature was lowered to 873 K. The POM reaction was started at this temperature using a methane–air feed (CH_4:O_2 ratio of 2) with a constant GHSV of 24,640 h^{-1} per reactor. After approximately 10 h on stream, the temperature was increased in the reaction feed to 1073 K in 100 K increments. The reaction was studied at each temperature for 10 h. A movable thermocouple inside each reactor was used to control temperature in the catalyst bed. The measured temperatures were close to the oven temperature (1073 ± 10 K) at the given space velocity. For brevity, we reported the temperatures of the heating system.

The feed components and the reaction products were analyzed by an online gas chromatograph (Agilent 7890) equipped with PLOT/Q (for CO_2) AL/S (for hydrocarbons) and Molsieve 5 (for H_2, O_2, N_2, and CO) columns as well as flame ionization and thermal conductivity detectors. The CH_4 conversion was calculated from the inlet and outlet concentrations of CH_4. The product selectivity was calculated on the feed basis. The GC analysis started after the system had reached reaction temperature and was carried out sequentially for each individual reactor.

2.4. Transient mechanistic experiments

Transient mechanistic analysis of the POM reaction was performed in the temporal analysis of products (TAP-2) reactor, a time-resolved technique with a resolution of approximately 100 μs. The TAP reactor system was described in detail elsewhere [22–24]. These experiments were carried out with differently treated catalysts: (i) fresh, (ii) pre-reduced in a flow of 10% H_2 in N_2 at 1073 K for 30 min, and (iii) used in the POM reaction for 120 h on stream. The catalytic materials (sieve fraction of 250–500 μm) were packed into the quartz micro reactor (i.d. = 6 mm, length = 40 mm) as a thin layer between two layers of quartz particles (sieve fraction of 250–350 μm) within the isothermal zone of the reactor. Since 3Ni_0.005Rh and 0.005Rh showed remarkably higher activity compared to 3Ni, catalyst weights were 50 mg for 3Ni and 30 mg for the Rh-containing samples in order to avoid complete conversions of feed components. The packed beds were 2.1 and 1.3 mm thick for the pure Ni and the Rh-containing catalysts, respectively. The catalyst reduction in H_2 was performed at ambient pressure followed by reactor evacuation to ca. 10^{-5} Pa as required for the transient experiments. The overall pulse size amounted to approximately 10^{15} molecules. Under these conditions, any collisions between gas-phase species are minimized (Knudsen diffusion regime). In other words, we analyzed pure heterogeneous reaction steps. Two types of transient experiments were performed at 1073 K:

- In order to estimate the catalyst activity for methane decomposition, single CH_4:Xe = 1:1 pulse experiments were carried out.
- The effect of O_2 on the kinetics of products formation was investigated by single O_2:CH_4:Ar = 1:1:1 pulse experiments.

The reaction mixtures were prepared using Ar (99.9990%), O_2 (99.995%), and CH_4 (99.95%) without additional purification. A quadrupole mass spectrometer (HAL RC 301 Hiden Analytical) was applied for quantitative analysis of reactants and reaction products. The following atomic mass units (AMUs) were used for mass-spectrometric identification of different compounds: 44 (CO_2), 40 (Ar), 32 (O_2), 28 (CO, CO_2), 18 (H_2O), 15 (CH_4), and 2 (H_2, CH_4). Pulses were repeated 10 times for each AMU and averaged to improve the signal-to-noise ratio. The concentration of feed components and reaction products was determined from the respective AMUs using standard fragmentation patterns and sensitivity factors. The contributions of CO_2 and CH_4 were subtracted from the signals of CO and H_2, respectively. H_2O could not be quantified properly in our experiments because of a bad signal-to-noise ratio.

3. Results

3.1. Physico-chemical properties of NiO_x–RhO_x/Al_2O_3 catalysts

The specific surface areas (S_{BET}) of the catalytic materials are shown in Table 1. They are in the range of 103–121 m^2 g^{-1}. No diffractional features indicating the presence of crystalline NiO or metallic Ni were identified in the XRD patterns of all fresh Ni-containing materials (diffractograms are presented in Fig. S1 in the supporting information). The absence of crystalline Ni-containing species may be understood either as the presence of small crystalline nanoparticles (<4 nm) or as surface $NiAl_xO_y$ species that cannot be detected by XRD due to the absence of long-range order. The detected reflections in the fresh materials were ascribed to γ-Al_2O_3, which, however, are hard to be distinguished from those of spinel type structure of nickel aluminate. An additional reflection appeared at $2\theta = 44.5^\circ$ in the XRD patterns of the bi-metallic catalysts having been used in the POM reaction according to the protocol described in Section 2.3. It was ascribed to metallic nickel. In other words, Ni^{2+} species were reduced to Ni during the course of the POM reaction. Compared to the bi-metallic catalysts, metallic nickel was not identified in the XRD patters of 3Ni_ used. These results demonstrate that the presence of Rh is an important requirement for the reaction-induced reduction of Ni^{2+} to Ni. Due to its low amount (⩽0.15 wt.%), Rh species were not detected by XRD.

UV/Vis-DR spectroscopy was applied to derive further insights into the state of nickel and rhodium species in the fresh samples.

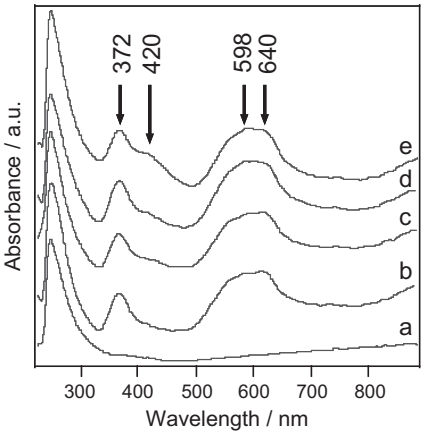

Fig. 1. UV/Vis-DR spectra of: (a) 0.03Rh, (b) 3Ni, (c) 3Ni_0.005Rh, (d) 3Ni_0.03Rh, and (e) 3Ni_0.15Rh.

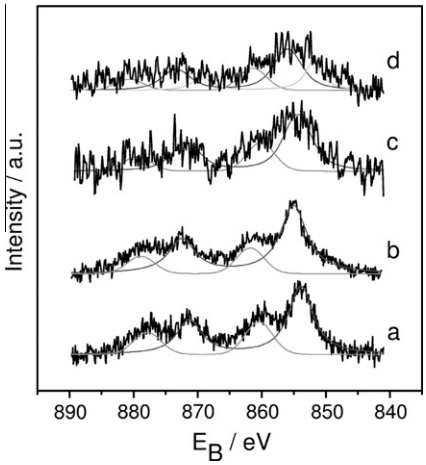

Fig. 2. XP spectra of: (a) 3Ni, (b) 3Ni_0.005Rh, (c) 3Ni_used, and (d) 3Ni_0.005Rh_used.

Fig. 1 compares the obtained spectra of 3Ni, 0.03Rh, and Ni–Rh materials with different Rh loadings. The mono-metallic materials were used as references in order to unambiguously identify the contributions of NiO_x and RhO_x species toward absorption of the bi-metallic materials. The UV/Vis-DR spectrum of 3Ni is characterized by three absorption bands at 372, 598, and 640 nm. According to literature [25–27], these bands can be assigned to the absorption of Ni^{2+} species within a spinel structure. Specifically, the absorption at 598 and 640 nm is characteristic for Ni^{2+} species in a tetrahedral environment, while octahedrally coordinated Ni^{2+} species absorb at 372 nm. Absorption below 300 nm might arise from free NiO species [25], which could not be identified by our XRD analysis. No absorption bands in the range from 300 to 800 nm were observed in the UV/Vis-DR spectrum of 0.03Rh. This is also valid for other mono-metallic Rh-containing samples. The spectrum of the highest loaded material (0.15Rh) is characterized by a broad band of fluorescence covering the whole range of wavelengths investigated.

In bi-metallic materials, the position and the intensity of the Ni^{2+} absorption bands discussed above were not influenced by the presence of Rh. However, an additional absorption band appeared at 420 nm. Significantly, its intensity increases with rhodium loading (3Ni_0.005Rh < 3Ni_0.03Rh < 3Ni_0.15Rh). Since this band only exists in the bi-metallic catalysts and develops with Rh loading, it should originate from an interaction between nickel and rhodium species. According to [28], this interaction is most likely a result of a so-called intervalence bonding, i.e., electron transitions between the d orbitals of both metals.

The above discussion was related to the bulk properties of materials. Nevertheless, the catalytic processes occur on their surfaces. Therefore, we analyzed the near-to-surface composition of our materials by ex situ XPS. The XP spectra of the $Ni2p_{3/2}$ region of fresh 3Ni and 3Ni_0.005Rh, as well as 3Ni_ used and 3Ni_0.005Rh_ used are compared in Fig. 2. Both fresh materials feature the satellite structure in their XP spectra being typical for Ni^{2+}. $Ni2p_{3/2}$ electron binding energy (E_B) in 3Ni was identified at 853.9 eV, which is in agreement with previous literature data [29]. Promoting this catalyst with 0.005 wt.%, Rh results in shifting of the $Ni2p_{3/2}$ peak to higher E_B (855.0 eV). However, upon further increasing Rh loading, this E_B value shifts back to 853.9 eV. In order to check whether the E_B shift of the $Ni2p_{3/2}$ signal in 3Ni_0.005Rh could be related to a change in the oxidation state of nickel, we calculated the modified Auger parameter α [21] according to Eq. (1). The α values were 1699.6 and 1699.9 for 3Ni and 3Ni_0.005Rh, respectively. Since these values are very close, we concluded that the oxidation state of nickel species did not depend on Rh loading and was equal to 2+. Taking into account the above discussion and the catalytic data presented in Section 3.2, the following explanation is suggested for the shift of the $Ni2p_{3/2}$ peak in 3Ni_0.005Rh. Our UV/Vis-DR analysis showed that rhodium and nickel species in all bi-metallic catalysts investigated interact with each other on an electronic level (Fig. 1). As Rh has a higher electronegativity than Ni, we assume that RhO_x species located near to $NiAl_xO_y$ species cause a change in the polarization of the electron density of Ni^{2+} (without changing the oxidation state). As a result, E_B of the $Ni2p_{3/2}$ electrons is shifted to higher values compared to non-effected Ni^{2+}. However, this phenomenon manifests itself at the Rh loading of 0.005 wt.%, while no shifting was observed in higher-loaded bi-metallic materials. This may be related to the nature of RhO_x species that depends on rhodium loading. Based on the very low apparent density of rhodium (0.0025 Rh nm^{-2}) on 3Ni_0.005Rh, this catalyst probably possesses near-to-isolated RhO_x species. We assume that the polarization effect of Rh on the electron density in Ni^{2+} decreases with an increasing degree of oligomerization of RhO_x species.

It is worth mentioning that the E_B value of the $Ni2p_{3/2}$ peak in 3Ni_0.005Rh_ used is also shifted to higher energies compared to the 3Ni_ used catalyst. Furthermore, the XP spectrum of 3Ni_0.005Rh_ used features a shoulder around 852.0 eV. Such signal was identified in all used Rh-containing bi-metallic materials. To assign this new nickel species, we recorded XP spectra of catalysts having been pre-reduced in a flow of H_2 (10% H_2 in Ar) at 1073 K for 30 min (3Ni_red and 3Ni_0.005Rh_red). In addition to signals related to Ni^{2+}, their XP spectra are characterized by a shoulder at 851.5 eV. Notwithstanding, this E_B value is about 1 eV lower than that for pure metallic nickel. E_B values around 852 eV are reported for Ni alloy with noble metals (e.g., with Au in [30]) or as Ni^0 intermixed with oxides [31]. An experimental uncertainty around 0.5 eV could be assumed in determining the accurate E_B due to the overlapping of more than one state in the reduced samples. Finally, we can conclude that in contrast to the mono-metallic 3Ni catalyst, metallic nickel species are formed in all bi-metallic catalysts under POM conditions.

3.2. Catalytic performance

In order to estimate the effect of Rh on the activity and time-on-stream stability of NiO_x(3 wt.%)/Al_2O_3 in the POM reaction, we performed catalytic tests at different temperatures as described in Section 2.3. It should be particularly stressed that no reductive

pretreatment was performed before the POM tests. Fig. 3a compares the degree of methane conversion over 3Ni, 0.005Rh, and 3Ni_0.005Rh at different temperatures over approximately 120 h on stream. No visible catalyst deactivation could be observed in these experiments. This is also valid for bi-metallic materials with higher Rh loadings. Their CH_4 conversion and selectivity toward CO, CO_2, and H_2 are summarized in Table 2. Since the materials studied did not show any significant deactivation, this table compares the average of all data points acquired at individual temperatures in the first and second cycles of experiment.

Fig. 3a illustrates that a methane conversion of approximately 5% was achieved over 3Ni, 0.005Rh, and 3Ni_0.005Rh at 873 K within the first cycle of experiment. As expected, the conversion increased with temperature. However, this increase depended on the catalyst. 3Ni_0.005Rh showed the highest conversion at 1073 K. It is also important to highlight that the conversion of methane over this catalyst strongly increased over 12 h on stream at this temperature (Fig. 3a). Since the catalyst temperature was constant during this reaction time, such temporal increase in the conversion should be due to reaction-induced changes in the catalyst structure. Mono- and bi-metallic catalysts possessing Rh loadings higher than 0.005 wt.% catalyzed the POM reaction to equilibrium from the beginning at each temperature. This explains why no such activation behavior was observed over these materials.

In order to elucidate whether this activation of 3Ni_0.005Rh is an irreversible process, we reduced the reaction temperature from 1073 K to 873 K in inert gas flow and repeated the catalytic test (second cycle) according to the protocol described in Section 2.3. A methane conversion of 50% was achieved over 3Ni_0.005Rh at 873 K in this second cycle. For comparison, the conversion in the first cycle was only 5% (first 12 h on stream in Fig. 3a). In other words, the 3Ni_0.005Rh catalyst was activated during the POM reaction above 873 K in the first cycle. However, no such activation was observed for the mono-metallic 3Ni and 0.005Rh catalysts. Both in the first and second cycles, they showed a methane conversion of only 5% at 873 K. These materials turned out to be rather inactive even at 1073 K in the second cycle. In contrast, 3Ni_0.005Rh exhibited at 1073 K near-to-equilibrium CH_4 conversion as well as CO and H_2 selectivity (Table 2). Moreover, the methane conversion achieved over this catalyst was higher than the sum of conversions over 3Ni and 0.005Rh, i.e., traces of Rh have a synergetic rather than a cumulative effect on the catalytic performance of NiO_x(3 wt.%)/Al_2O_3. From this table, it is also clearly seen that mono-metallic Rh materials with high ($\geqslant$0.03 wt.%) loadings perform similar to the respective bi-metallic ones and to 3Ni_0.005Rh with the latter possessing a Rh loading, which is one order of magnitude lower.

The above results raise the question, whether the catalytic performance of 3Ni, 0.005Rh, and 3Ni_0.005Rh is influenced by the reduction degree of metals. Therefore, we reduced the fresh catalytic materials at 1073 K as described in Section 2.3, directly followed by investigating the POM reaction at 873, 973, and 1073 K. The achieved methane conversion and product selectivity are presented in Fig. 3b and Table 2, respectively. As expected, the reduced catalysts showed high methane conversion starting from 873 K. Their POM performance was significantly superior to that of the fresh ones. Among the reduced catalysts, the highest methane conversion and product selectivity was achieved over the 3Ni_0.005Rh_red catalyst, while 0.005Rh_red showed the lowest activity. This is most probably due to the very low amount of Rh per mass unit of the latter catalyst. The activity of the 3Ni_red catalyst was scarcely lower than that of the reduced bi-metallic one. This leads to the conclusion that the catalytic performance of 3Ni_0.005Rh_red cannot be governed only by the noble metal. Another key result is the very similar POM performance of 3Ni_0.005Rh_red and 3Ni_0.005Rh having been activated directly under the reaction conditions at 1073 K (see second cycle in Fig. 3a). The effect of Rh on catalytic performance and activating behavior of bi-metallic Ni–Rh catalysts is discussed in Section 4, taking into account the results of mechanistic analysis presented below.

3.3. Mechanistic analysis of the POM reaction

In order to elucidate the effects of individual metals, their state (oxidized vs. reduced) and the presence of O_2 on methane oxidation to CO, CO_2, and H_2, we analyzed transient experiments on CH_4 and CH_4–O_2 interactions with fresh, used, and reduced mono- and bi-metallic catalysts. For investigation of synergism of Ni and Rh, it is essential to exclude the latter to be alone responsible for catalytic activity and selectivity. For this reason, we studied the catalysts containing the lowest Rh amount of 0.005 wt.%. An overall apparent constant (k_{CH_4}) of methane oxidation was estimated by applying the so-called thin-zone TAP reactor model [32] for evaluation of CH_4 and CH_4–O_2 pulse experiments over fresh and reduced catalysts (Eq. (2)). The constants derived are summarized in Fig. 4.

$$X = \frac{k_{CH_4} \cdot \varepsilon_b \cdot (\Delta L \cdot L_{II}/D_e)}{1 + k_{CH_4} \cdot \varepsilon_b \cdot (\Delta L \cdot L_{II}/D_e)} \quad (2)$$

where X and k_{CH_4} are the conversion of methane and the corresponding apparent constant. ΔL and L_{II} are lengths of the catalyst layer and the second inert zone, respectively. D_e is an effective diffusion coefficient of methane. ε_b is the fractional voidage of the packed bed in the reactor.

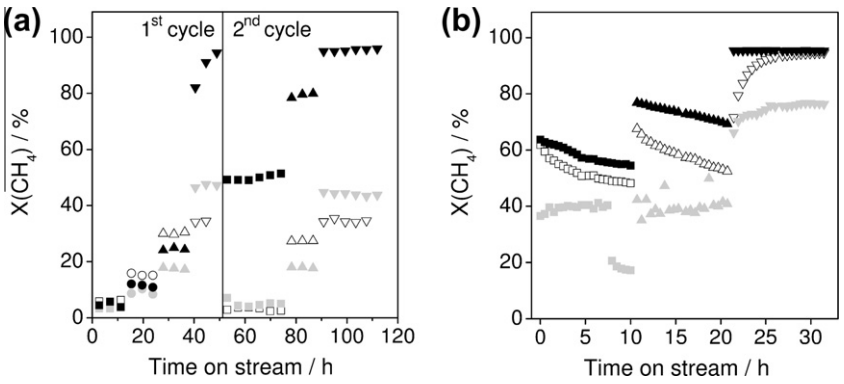

Fig. 3. Conversion of CH_4 over 3Ni (white), 0.005Rh (gray), and 3Ni_0.005Rh (black) at 873 (□, ■, ■), 923 (○, ●, ●), 973 (△, ▲, ▲), and 1073 K (▽, ▼, ▼) using a reaction feed consisting of 29% methane in air with a constant gas-hourly space velocity (GHSV) of 24,640 h^{-1}. Panels (a) and (b) represent methane conversion over fresh and pre-reduced catalysts, respectively.

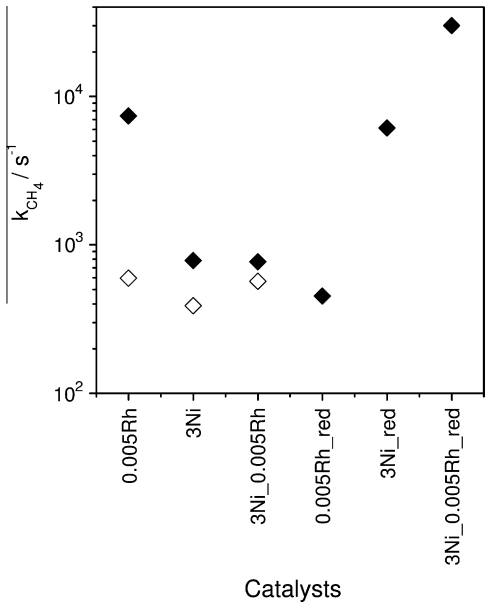

Fig. 4. Apparent constants of methane oxidation from CH_4 (open symbols) and CH_4–O_2 (closed symbols) pulse experiments at 1073 K.

The following relative activity order was obtained for O_2-free CH_4 oxidation over fresh catalysts containing RhO_x and $NiAl_xO_y$: 3Ni_0.005Rh > 0.005Rh > 3Ni, respectively. As evident from Fig. 4, the constants of CH_4 oxidation increased when CH_4 was oxidized over these catalysts in the presence of O_2 indicating that oxygen species formed from gas-phase O_2 accelerate the CH_4 oxidation. Among the catalysts studied, 3Ni showed the lowest activity, while 0.005Rh was the most active catalyst. The latter catalyst became less active after reduction in an H_2 (10% H_2 in N_2) flow at 1073 K for 30 min. In other words, RhO_x species are considerably more active for CH_4 oxidation in the presence of O_2 than metallic Rh. Contrarily, reduced Ni species showed the higher activity compared to $NiAl_xO_y$ (Fig. 4). It is important to highlight that the apparent constant of CH_4 oxidation was the highest over 3Ni_0.005Rh_red and larger than the sum of the corresponding constants over 3Ni_red and 0.005Rh_red. This is an indirect support for a synergy effect of Ni and Rh of the bi-metallic catalyst.

CO_2, CO, and H_2 were observed when CH_4 was pulsed over fresh 3Ni, 0.005Rh, and 3Ni_0.005Rh at 1073 K. The presence of oxygen-containing products proves the ability of lattice oxygen from $NiAl_xO_y$ and RhO_x to oxidize CH_4. The same products were also identified when CH_4 was oxidized in the presence of gas-phase O_2. Fig. 5 exemplifies transient responses of CO, CO_2, and H_2 after CH_4 and CH_4–O_2 pulsing at 1073 K over fresh 3Ni_0.005Rh. The transients of feed components are presented in Fig. S2 in the supporting information. Since these reaction products (H_2, CO, and CO_2) differ significantly in their molecular weights and, hence, in their diffusion coefficients, the time scale in this figure was normalized according to Eq. (3). This normalization is based on the theory of the TAP reactor developed by Yablonsky et al. [22,33,34]. Fig. 5 also contains the transients of Ar and Xe, which are characteristic of simple diffusion through the reactor. This enables a clear demonstration of the effect of chemical reaction(s) on the shape of transients of reaction products. Since the transient experiments were performed in a three-zone reactor (1st zone – SiO_2 particles, 2nd zone – catalyst, 3rd zone – SiO_2 particles), we recalculated the Ar response from the experimental one assuming Ar diffusion through a two-zone reactor (1st zone – catalyst and 2nd zone – SiO_2 particles). Figs. S3–S5 in the supporting information show experimental and simulated responses of inert gases. This calculation was very important because the reaction products were formed in the catalyst zone and diffused through this zone and the following zone of SiO_2 particles while inert gases diffused through the three zones.

$$t_{\text{normalized}} = t_{\text{experiment}} \cdot \sqrt{\frac{M_{\text{inert}}}{M_{\text{product}}}} \tag{3}$$

where M_{inert} and M_{product} are molecular weights of inert standard and gas-phase products, respectively. $t_{\text{experiment}}$ is the experimental time for this component.

As evident from Fig. 5, the transient responses of CO, CO_2, and H_2 are shifted to longer times compared to that of Ar or Xe proving that they are reaction products of CH_4 oxidation. However, the concentration of these products and the shapes of their responses are strongly influenced by the presence of O_2. Compared to O_2-free CH_4 oxidation, (i) CO_2 is the main product of methane oxidation and (ii) all transient responses are significantly narrower and shifted to shorter times when CH_4 and O_2 were pulsed together (Fig. 5). It is also clearly seen that the CO transient crosses the diffusion curve (Xe transient) when CH_4 was pulsed over the fresh catalysts, while it does not cross upon CH_4 oxidation in the presence of O_2. According to [22], the latter situation can be explained by the fact that CO is primarily formed from CH_4 followed by fast oxidation to CO_2. Actually, the higher concentration of CO_2 and the shifting of the CO_2 response to longer times compared to CO support this assumption. In summary, the results in Fig. 5 nicely show that the shape of CO, CO_2, and H_2 transients is very sensitive to the mode of CH_4 oxidation.

According to [22,35], $t_{\max}$ (the position of the signal maximum) and $t_{h/2}$ (the width at the signals half height) of transient responses

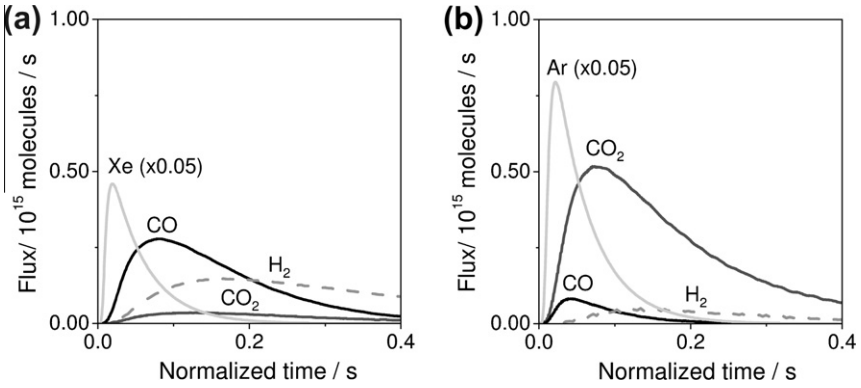

Fig. 5. Transient responses of the reaction products formed after pulsing of: (a) CH_4 (CH_4:Xe = 1:1) and (b) CH_4–O_2 (CH_4:O_2:Ar = 1:1:1) over fresh 3Ni_0.005Rh at 1073 K. Overall pulse size was 10^{15} molecules. Time was normalized according to Eq. (3).

of reaction products contain information about the kinetics of their formation and possible consecutive transformation(s) as well as about their diffusion through the reactor. In order to exclude the effect of diffusion on the t_{max} and $t_{h/2}$ values of CO, CO_2, and H_2, we subtracted from their values the corresponding values of the recalculated transients of inert gases (see Figs. S3–S5 in the supporting information). Such differences are related to the reaction kinetics and called as Δt_{max} and $\Delta t_{h/2}$ through the whole manuscript. Figs. 6 and 7 compare these values, respectively. When oxidizing CH_4 over the fresh catalysts in the absence and the presence of O_2, Δt_{max} and $\Delta t_{h/2}$ values follow the order $CO < CO_2 < H_2$. In other words, irrespective of the reaction mechanism, the formation of H_2 is by far the slowest reaction over all the catalysts studied. This is in agreement with previous studies of the POM reaction in the TAP reactor over a commercial Ni-based steam reforming catalyst [36] but contradicts to [37], where SiO_2- and Al_2O_3-supported Ni- and Ru-based catalysts were investigated. In the latter work, the authors, however, did not consider the effect of strongly different diffusion coefficients of H_2 and CO_x on their order of appearance in the TAP experiments.

Another important result from Figs. 6 and 7 is the fact that the Δt_{max} and $\Delta t_{h/2}$ values of CO, CO_2, and H_2 transients in the CH_4–O_2 experiments over fresh catalysts are smaller than those in the CH_4 tests. This means that the presence of oxygen accelerates the reaction pathways with participation of these products. With respect to the order of the Δt_{max} or $\Delta t_{h/2}$ values of CO and CO_2, the fresh catalysts can be ordered as follows: 0.005Rh > 3Ni > 3Ni0.005Rh. These results suggest that the rates of CO and CO_2 production (formation minus secondary transformations) are faster over the bi-metallic catalyst than over the respective mono-metallic counterparts. Actually, the above activity order agrees well with that of methane oxidation over the same catalysts at ambient pressure (Fig. 3a). This may give evidence of a new, unique catalytic behavior of the bi-metallic material, but also proves that such behavior is not due to combination of positive characteristics of individual metals.

A similar analysis of the Δt_{max} and $\Delta t_{h/2}$ of CO_2, CO, and H_2 was also performed for the CH_4–O_2 pulse experiments over 3Ni_red, 0.005Rh_red, and 3Ni_0.005Rh_red as well as over 3Ni_0.005Rh

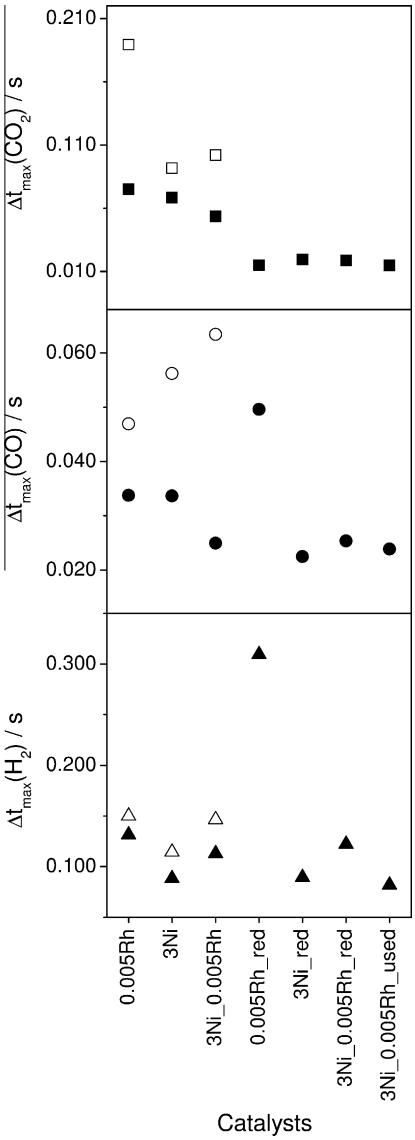

Fig. 6. Δt_{max} of transient response to CO_2, CO, and H_2 over different catalysts derived from CH_4 (open symbols) and CH_4–O_2 (closed symbols) pulse experiments at 1073 K.

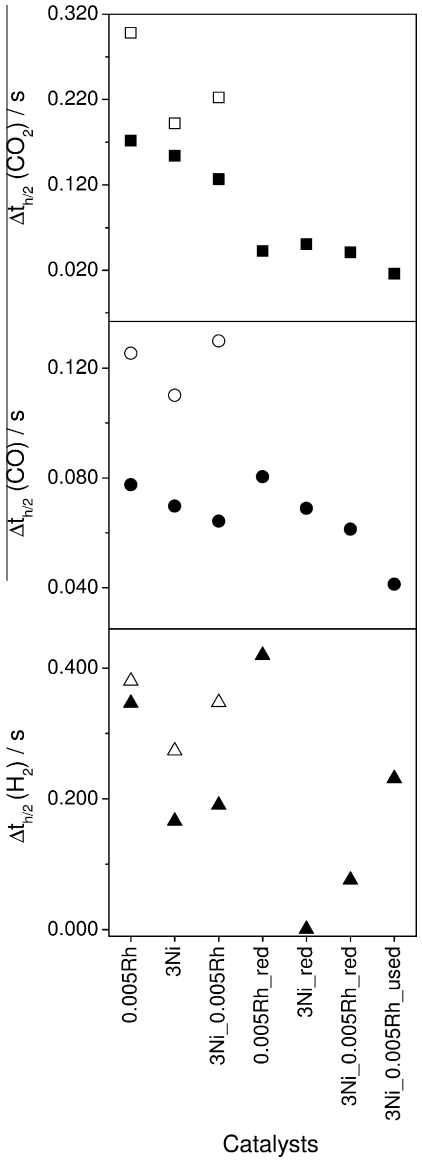

Fig. 7. $\Delta t_{h/2}$ of transient responses to CO_2, CO, and H_2 over different catalysts derived from CH_4 (open symbols) and CH_4–O_2 (closed symbols) pulse experiments at 1073 K.

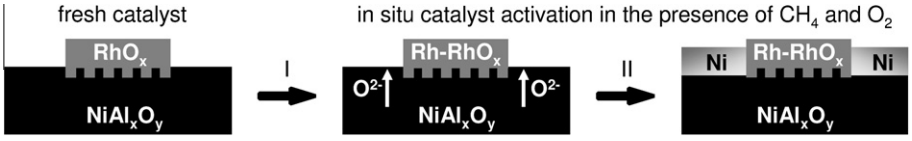

Fig. 8. Suggested mechanistic scheme of the synergetic effect of Rh on NiO_x(3 wt.%)/Al_2O_3 catalyst in the POM reaction.

having been used for 120 h under POM reaction conditions. The corresponding values are summarized in Figs. 6 and 7. As evidenced from lowering of the corresponding Δt_{max} values, reaction pathways of formation/transformation of CO and CO_2 are faster over the reduced Ni-containing samples compared to the fresh ones. Another important result to be highlighted is the order of appearance of CO_2 and CO. Compared to the Δt_{max} and $\Delta t_{h/2}$ values of CO_2, these parameters of CO over the reduced catalysts are approximately 2 times higher, while those over the fresh catalysts are significantly lower. Moreover, the Δt_{max} and $\Delta t_{h/2}$ values of CO_2 were reduced by a factor of approximately 5 when oxidizing CH_4 in presence of O_2 over the reduced catalysts. Based on these experimental results, we conclude that the overall scheme of methane oxidation is changed after reductive catalyst treatment. Such changes in the POM reaction mechanism were reported several times for different transition metals used as supported or bulk catalysts [38]. In contrast to the fresh catalysts, the reduced ones completely oxidize CH_4 followed by consecutive CO_2 conversion to CO. With respect to the H_2 formation, it is concluded that it does not originate via the same reaction pathways as CO, because the Δt_{max} values of CO and H_2 differ significantly.

Thus, the above mechanistic analysis clearly demonstrated that individual reaction pathways (kinetics and mechanism) are influenced by both individual metals (Rh vs. Ni) and their reduction degree. From a kinetic point of view, metallic Ni should be the active component catalyzing the POM reaction over reduced 3Ni_0.005Rh_red. The role of Rh loading in bi-metallic Rh–Ni materials is discussed in the following section.

4. Discussion

The results presented in Section 3.2 demonstrate a very low activity of fresh 3Ni in the POM reaction. According to previous studies [39,40], its poor activity is due to the fact that nickel is present as unreactive $NiAl_xO_y$ species. In general, to make nickel-containing materials active for the POM reaction, they have to be ex situ reduced in an H_2 flow to form metallic Ni [41]. The lower the Ni loading, the higher the reduction temperature is required due to the high stability of $NiAl_xO_y$. As demonstrated in the present study (Section 3.2), the reduction step can be avoided when promoting NiO_x(3 wt.%)/Al_2O_3 with small amounts of rhodium. Such bi-metallic catalysts are activated in situ under the POM conditions. Several previous studies reported on the promoting effect of noble metals on the catalytic performance of Ni-based catalysts in partial oxidation and steam reforming of methane [9–12]. From a mechanistic point of view, it was suggested that the presence of noble metals facilitates the formation of surface metallic nickel species via a hydrogen-spillover mechanism. The latter species catalyze the syngas production. However, this mechanistic concept has been developed for materials possessing Rh loading higher than 0.05 wt.%. No promoting effect of noble metals has been reported for catalysts with lower Rh contents. Contrarily, our study demonstrated that the activity of NiO_x(3 wt.%)/Al_2O_3 in the POM reaction strongly increased after its promotion with even 0.005 wt.% Rh, i.e., one order lower Rh amount than in the previous studies. Moreover, our Ni–Rh and Rh materials with Rh loading higher than 0.005 wt.% were similarly active, i.e., Ni and Rh showed a synergetic effect with respect to the POM activity and selectivity when the Rh loading was as low as 0.005 wt.%. Taking into account these differences and the results of our detailed mechanistic analysis, we suggest an alternative mechanistic concept of the promoting effect of Rh on in situ reduction of Ni^{2+} to Ni and on the POM performance.

Fig. 8 shows a simplified scheme of activation of bi-metallic materials under POM conditions. $NiAl_xO_y$ and RhO_x are main species in the fresh catalysts. As proven by transient experiments in Section 3.3, these species are able to oxidize methane in the absence of gas-phase oxygen. From a kinetic point of view, the apparent constant of CH_4 oxidation over RhO_x species is approximately 10 times higher than that over $NiAl_xO_y$ (Fig. 4). These results together with the noble nature of Rh enabled us to suggest that RhO_x is partially converted to metallic Rh in the POM feed at 1073 K (I in Fig. 8). These new species are also active for the formation of surface CH_x species from CH_4 in the absence and in the presence of adsorbed oxygen species [42,43]. These carbon-containing species can be converted to CO_x by gas-phase O_2 or surface oxygen species formed over rhodium species. Owing to the high reducing potential of CH_x species, they can also react with lattice oxygen of adjacent $NiAl_xO_y$ to yield reduced nickel species (II in Fig. 8). Depending on the kinetics of reduction and reoxidation of $NiAl_xO_y$, metallic Ni can be formed under POM conditions. This process is probably responsible for the increase in methane conversion from 82 to 95% over 3Ni_0.005Rh within first 10 h on POM stream at 1073 K (Fig. 3a). The CO selectivity increased from 86% to 91%, respectively. It is well accepted that metallic nickel is active and selective in the POM reaction [44–46]. In fact, our XPS and XRD analysis of materials used in the POM reaction proved the formation of metallic nickel in 3Ni_0.005Rh, while metallic nickel was not identified in 3Ni_ used. In other words, presence of Rh facilitated the conversion of Ni^{2+} to Ni. A similar effect of noble metals has been also reported for other metal oxides. For example, Pt supported over CeO_2-containing supports strongly increased the reduction degree of ceria upon oxygen-free oxidation of CO and H_2 [47–50]. Moreover, several authors [51,52] reported H_2-TPR data illustrating the process of reduction starting at lower temperatures over noble metal promoted compared to mono-metallic nickel-based materials.

Based on the above discussion and the POM performance of differently Rh-loaded bi- and mono-metallic materials (Fig. 3 and Table 2), it can be concluded that Rh fulfills a double role in the bi-metallic catalysts, which is determined by its loading. Irrespective of the loading, small amounts (<0.15 wt.%) of Rh help to in situ convert catalytically non-active $NiAl_xO_y$ to metallic Ni species. Owing to different intrinsic POM activity of Rh and Ni species, the performance of NiO_x–RhO_x/Al_2O_3 materials is determined by Rh if its loading is close to or higher than 0.03 wt.%. Otherwise, metallic Ni catalyzes the POM reaction.

5. Conclusions

We demonstrated that promoting NiO_x(3 wt.%)/Al_2O_3 with tiny amounts ($\geqslant$0.005 wt.%) of RhO_x resulted in active, selective, and stable catalysts for syngas production via partial oxidation of methane. In contrast to previously reported low-loaded Ni

catalysts, no reductive catalyst activation is required because promotion with rhodium facilitates the activation of bi-metallic catalysts in situ under POM conditions. Transient experiments in the TAP reactor in combination with catalyst characterization by XPS and UV/Vis-DR spectroscopy enabled us to reveal possible reasons of the rhodium promoting effect. Owing to the high intrinsic activity of RhO_x species for methane oxidation, they are reduced to metallic Rh species during the course of the POM reaction. These new species catalyze in situ transformation of inactive $NiAl_xO_y$ to metallic Ni species. The latter are responsible for the syngas production. However, the contribution of the nickel species to the target reaction decreases with an increase in rhodium loading from 0.005 to 0.15 wt.% due to the higher activity of metallic rhodium species compared to that of nickel ones.

Acknowledgments

Dr. Vita Kondratenko and Leif Knoepke are gratefully acknowledged for helpful discussion and experimental input.

Appendix A. Supplementary material

Supplementary data associated with this article can be found, in the online version, at doi:10.1016/j.jcat.2011.03.010.

References

[1] J. Sauer, M. Bewersdorf, M. Köstner, M. Rinner, D. Wolf, in: G. Ertl, H. Knözinger, F. Schüth, J. Weitkamp (Eds.), Handbook of Heterogeneous Catalysis, vol. 5, Wiley-VCH Verlag GmbH & Co., KGaA Weinheim, 2008, p. 2592.
[2] G.J. Thomas, K.J. Mitchell, GB 1159035 (A), 1969 (to ICI LTD).
[3] H. Pichler, in: W.G. Frankenburg, V.I. Komarewsky, E.K. Rideal (Eds.), Advances in Catalysis, vol. 4, Academic Press, 1952, p. 271.
[4] J. Sehested, Catal. Today 111 (2006) 103.
[5] B.C. Enger, R. Lodeng, A. Holmen, Appl. Catal. A 346 (2008) 1.
[6] P.F.v.d. Oosterkamp, in: I. Horvath (Ed.), Encyclopedia of Catalysis, vol. 6, John Wiley & Sons, Weinheim, 2003, p. 770.
[7] D. Li, K. Nishida, Y. Zhan, T. Shishido, Y. Oumi, T. Sano, K. Takehira, Appl. Catal. A 350 (2008) 225.
[8] K. Nakagawa, N. Ikenaga, Y. Teng, T. Kobayashi, T. Suzuki, Appl. Catal. A 180 (1999) 183.
[9] F. Basile, G. Fornasari, F. Trifirò, A. Vaccari, Catal. Today 77 (2002) 215.
[10] L.P.R. Profeti, J.A.C. Dias, J.M. Assaf, E.M. Assaf, J. Power Sources 190 (2009) 525.
[11] D. Li, T. Shishido, Y. Oumi, T. Sano, K. Takehira, Appl. Catal. A 332 (2007) 98.
[12] D. Li, I. Atake, T. Shishido, Y. Oumi, T. Sano, K. Takehira, J. Catal. 250 (2007) 299.
[13] Y.-G. Chen, K. Tomishige, K. Yokoyama, K. Fujimoto, Appl. Catal. A 165 (1997) 335.
[14] C. Crisafulli, S. Scirè, R. Maggiore, S. Minicò, S. Galvagno, Catal. Lett. 59 (1999) 21.
[15] B. Enger, R. Lødeng, A. Holmen, Catal. Lett. 134 (2010) 13.
[16] J. Perez-Ramirez, E.V. Kondratenko, V.A. Kondratenko, M. Baerns, J. Catal. 227 (2004) 90.
[17] J. Perez-Ramirez, E.V. Kondratenko, V.A. Kondratenko, M. Baerns, J. Catal. 229 (2005) 303.
[18] V.A. Kondratenko, G. Weinberg, M.-M. Pohl, D.S. Su, Appl. Catal. A 381 (2010) 66.
[19] V.A. Kondratenko, Appl. Catal. A 381 (2010) 74.
[20] R.L. Augustine, Incipient wetness, in: Heterogeneous Catalysis for the Synthetic Chemist, Marcel Dekker, Inc., New York, 1996, p. 287.
[21] C.D. Wagmer, L.H. Gale, R.H. Raymond, Anal. Chem. 51 (1977) 466.
[22] J.T. Gleaves, G.S. Yablonskii, P. Phanawadee, Y. Schuurman, Appl. Catal. A 160 (1997) 55.
[23] J. Pérez-Ramírez, E.V. Kondratenko, Catal. Today 121 (2007) 160.
[24] E.V. Kondratenko, Catal. Today 157 (2010) 16.
[25] A. Cimino, M. Lo Jacono, M. Schiavello, J. Phys. Chem. 75 (1971) 1044.
[26] P. Kim, Y. Kim, H. Kim, I.K. Song, J. Yi, Appl. Catal. A 272 (2004) 157.
[27] D. Schmitz Du Mont, A. Lule, D. Reinen, Ber. Bunsenges. Phys. Chem. 69 (1965).
[28] Z. Sojka, F. Bozon-Verduraz, M. Che, in: G. Ertl, H. Knözinger, F. Schüth, J. Weitkamp (Eds.), Handbook of Heterogeneous Catalysis, vol. 2, WILEY-VCH Verlag GmbH & Co., KGaA, Weinheim, 2008, p. 1039.
[29] J.F. Moulder, W.F. Stickle, P.E. Sobol, K.D. Bomben, Handbook of X Ray Photoelectron Spectroscopy: A Reference Book of Standard Spectra for Identification and Interpretation of Xps Data, Physical Electronics, 1995.
[30] F.U. Hillebrecht, J.C. Fuggle, P.A. Bennett, Z. Zolstroknierek, C. Freiburg, Phys. Rev. B 27 (1983) 2145.
[31] A.R. González-Elipe, G. Munuera, J.P. Espinos, J.M. Sanz, Surf. Sci. 220 (1989) 368.
[32] J.T. Gleaves, G. Yablonsky, X. Zheng, R. Fushimi, P.L. Mills, J. Mol. Catal. A 315 (2010) 108.
[33] G.S. Yablonsky, D. Constales, S.O. Shekhtman, J.T. Gleaves, Chem. Eng. Sci. 62 (2007) 6754.
[34] G.S. Yablonsky, M. Olea, G.B. Marin, J. Catal. 216 (2003) 120.
[35] J. Pérez-Ramírez, E.V. Kondratenko, J. Catal. 250 (2007) 240.
[36] E.V. Kondratenko, H. Wang, V.A. Kondratenko, J. Caro, J. Mol. Catal. A 297 (2009) 142.
[37] Y. Schuurman, C. Marquez-Alvarez, V.C.H. Kroll, C. Mirodatos, Catal. Today 46 (1998) 185.
[38] T.V. Choudhary, V.R. Choudhary, Angew. Chem. Int. Ed. 47 (2008) 1828.
[39] O. Dewaele, G.F. Froment, J. Catal. 184 (1999) 499.
[40] C. Berger-Karin, E.V. Kondratenko, Stud. Surf. Sci. Catal. 175 (2010) 635.
[41] K. Huszar, G. Racz, G. Szekely, Acta Chim. Hung. 70 (1971) 287.
[42] M. Fathi, F. Monnet, Y. Schuurman, A. Holmen, C. Mirodatos, J. Catal. 190 (2000) 439.
[43] O.V. Buyevskaya, D. Wolf, M. Baerns, Catal. Lett. 29 (1994) 249.
[44] M.A. Goula, A.A. Lemonidou, W. Grünert, M. Baerns, Catal. Today 32 (1996) 149.
[45] Å. Slagtern, H.M. Swaan, U. Olsbye, I.M. Dahl, C. Mirodatos, Catal. Today 46 (1998) 107.
[46] R. Jin, Y. Chen, W. Li, W. Cui, Y. Ji, C. Yu, Y. Jiang, Appl. Catal. A 201 (2000) 71.
[47] T. Tanabe, A. Suda, C. Descorme, D. Duprez, H. Shinjoh, M. Sugiura, Stud. Surf. Sci. Catal. 138 (2001) 135.
[48] A. Suda, K. Yamamura, H. Sobukawa, Y. Ukyo, T. Tanabe, Y. Nagai, F. Dong, M. Sugiura, J. Ceram. Soc. Jpn. 112 (2004) 623.
[49] E.V. Kondratenko, Y. Sakamoto, K. Okumura, H. Shinjoh, Appl. Catal. B 89 (2009) 476.
[50] E. V. Kondratenko, Y. Sakamoto, K. Okumura, H. Shinjoh, Catal. Today. doi:10.1016/j.cattod.2010.10.015.
[51] C. Li, Y.W. Chen, Thermochim. Acta 256 (1995) 457.
[52] Z. Hou, T. Yashima, Catal. Lett. 89 (2003) 193.